Hydraulic Fracture Stimulated Zone Analysis with a FEM Upscaled Model

Erfan Sarvaramini [a]*, Robert Gracie[a], and Maurice. Dusseault[b]

[a] *Department of Civil and Environmental Engineering, University of Waterloo, Ontario, Canada*
[b] *Department of Earth and Environmental Sciences, University of Waterloo, Ontario, Canada*
*esarvaramini@uwaterloo.ca

Abstract

The development of a stimulated volume during hydraulic fracturing in a naturally fractured rock mass is singularly challenging to simulate mathematically. At the discrete level there are strong fabric issues (oriented joint sets, perhaps faults, and weak bedding planes), different joint properties, Biot coupling, advective-conductive heat transfer, and flow in joint arrays with changing apertures. Complex discrete interaction laws for joints involve sliding Mohr-Coulomb friction with joint dilation (i.e. aperture increase), cohesion loss related to sliding and to extensional displacements across joints, strongly non-linear block contact stiffness behavior that deviates from Hertzian behavior, and loss of contacts during hydraulic fracturing when some natural fractures become non-contacting. Furthermore, the rock blocks delineated by the joints in the stimulated volume possess anisotropic properties, and large-scale heterogeneity also exists. A novel upscaled HF model for stimulated volume simulation of a naturally fractured rock has been developed using a typical Galerkin Finite Element Method approach with full Biot coupling, but using a non-local plasticity formulation with dilation to track the evolution of bulk stiffness and fluid transmission properties. First, the evolution of the stimulated volume is quantified for an example of a 3D hydraulic fracturing propagation in the naturally fractured rock. After creation of a sufficiently large stimulated volume the well is shut-in and pressure is allowed to fall-off. We use the pressure decline analysis to relate the post shut-in behavior of the stimulated volume to the geomechanics of fracturing. Preliminary results are promising: we will show interesting results that show this approach may be highly useful in analyzing hydraulic fracturing data and incorporating damage mechanics approaches into design in geomaterials.

Keywords: Hydraulic Fracturing, Stimulated Volume, Naturally Fractured Rocks, Finite Element Analysis

1. Introduction

It is generally understood that hydraulic fracturing (HF) in the naturally fractured rocks does not lead to creation of a single fracture, rather it creates a Stimulated Volume (SV) of enhanced permeability through reactivation of the pre-existing natural fractures, tensile fracturing, irreversible plastic deformation and damaging of the bulk (Cipolla et al., 2010 and Mayerhofer et al., 2010). However, the simulation of the evolution of the SV is an intricate task because of the considerable uncertainty with respect to the shape, size, and conductivity of the stimulated volume, as these characteristics are strongly

dependent upon the distribution of natural fractures, in-situ stresses, and other reservoir and fluid parameters. Microseismic imaging is commonly used to estimate the extent of the complex hydraulic fracturing and SV evolution in hydraulically stimulated tight formations (Maxwell, 2014, Dusseault et al. 2011). Microseismic measures the seismic energy release associated with shear slippage along the natural fractures and weakness planes (i.e., Mode II and Mode III fracturing). The shear fracturing effects result in a stimulated region of naturally self-propped fractures (i.e., a shear dilation zone) spanning a large volume of the target reservoir formation (Fig. 1) (Dusseault, 2013). The size of the micorsiemic clouds is often implicitly related to the extent of the SV and shear dilation zone. However, microsiemic provides no specific links to mechanical properties, jointed rock fabrics, dynamic of fracturing, and SV conductivity. Therefore, it is important to develop a geomechanical model which is capable in constraining the extent of the SV leading to a more consistent interpretation of the microsiemic data.

HF operation in a naturally fractured rock masses also creates Mode I tensile fractures that will propagate preferentially along the local rock fabric, as they possess far lower fracture toughness values than the dense, strong rock matrix. The path of fracturing; however, can change due to the stress alteration near the leading edge of the tensile fracture resulting in fracture bifurcation. On a larger scale than the local fracture fabrics, fractures will propagate perpendicular to the direction of the minimum in-situ stress. This portion of the SV, which is mostly dominated by Mode I fracturing, is called the "sand" zone because it is the zone that can be propped with injected sand (Fig. 1).

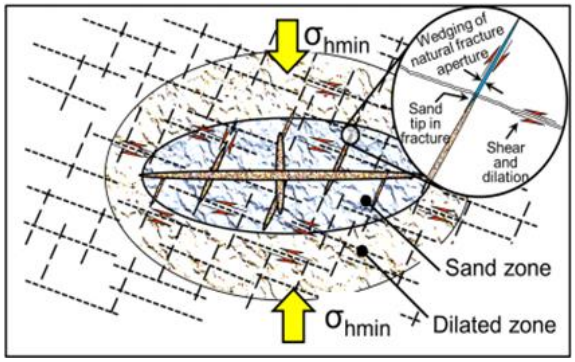

Fig. 1 The various stimulated zones during injection into a naturally fractured system (Dusseault, 2013)

In this study, we neglect the details of the complex fracturing at the discrete level, and instead, the SV in the jointed rock mass is represented by an equivalent smeared poro-elastic-plastic continuum zone of enhanced permeability. The details of the complex fracturing, nucleation and micro-events of void coalescence in the discrete level are translated into three constitutive models: (1) for the degradation of the yield strength of rock (plastic softening), (2) for the evolution of effective permeability with plasticity, and (3) for the energy dissipation within the localization band, which is controlled by an internal characteristic length scale. The latter is related to the natural fracture distribution and spacing as well as the micromechanics of deformation. A Drucker-Prager (DP) model (Drucker and Prager,

1952) is implemented within a poro-elastic-plastic Finite Element Method (FEM) framework based on Biot's theory (Biot, 1941). The DP failure criterion is capable to describe the Mode I and Mode II or III fracturing behavior in geomaterials.

In the next step, the pressure fall-off period after the shut-in moment is analyzed to quantify the various flow regimes and fracturing parameters. For this purpose, we will use the pressure and pressure derivative diagnostic plot commonly used for draw-down and build-up well-testing interpretations. One of the main objectives of this study is to construct a mathematical tool for the hydraulic fracture simulation of both SV and post shut-in. This methodology is expected to provide more insights on how the post-fracturing behavior of a fractured well can be related to the natural fracture distribution and micro-mechanics of damage and plasticity in the effective localized dilation zone.

2. Mathematical formulation

The poro-elasto-plastic domain of the problem is depicted in Fig 2. The domain is bounded by its boundary $\partial\Omega$ which is composed of the sets of prescribed displacements $\partial\Omega_u$, traction $\partial\Omega_t$, flow rate $\partial\Omega_q$, pressure and plastic strain $\partial\Omega_\varrho$. The behavior of the body subjected to the given boundary conditions is described by the following equations:

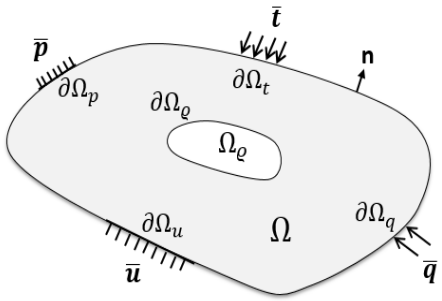

Fig. 2. Schematic of the problem domain

2.1 Equilibrium equation

The equilibrium equation and boundary conditions for the system described in Fig. 2 are

$$\nabla.(\boldsymbol{\sigma}' - \alpha p\mathbf{I}) = 0, \tag{1}$$

and

$$\boldsymbol{\sigma}'.\mathbf{n}\ (\text{on}\ \partial\Omega_t) = \bar{\mathbf{t}}\ ,\mathbf{u}(\text{on}\ \partial\Omega_u) = \bar{\mathbf{u}}, \tag{2}$$

in which σ ' is the Cauchy effective stress tensor, α is the Biot's coefficient, p is the fluid pressure, I is the identity tensor, and $\bar{\mathbf{t}}$ and $\bar{\mathbf{u}}$ are the prescribed traction and displacement on the boundary $\partial\Omega_t$ and $\partial\Omega_u$, respectively. Using the Hook's law, we have

$$\boldsymbol{\sigma}' = \mathbf{C}: \boldsymbol{\varepsilon}_e, \tag{3}$$

where $\boldsymbol{\varepsilon}_e$ is the elastic strain tensor and $\mathbf{C}$ is the fourth-order stiffness tensor. The elastic component in (3) can be expressed as

$$\boldsymbol{\varepsilon}_e = \boldsymbol{\varepsilon} - \boldsymbol{\varepsilon}_p. \tag{4}$$

In which $\boldsymbol{\varepsilon}$ is the total strain tensor and $\boldsymbol{\varepsilon}_p$ is the plastic strain tensor. The amount of plastic strain can be determined using an associate plastic flow rule as:

$$\boldsymbol{\Delta\varepsilon}_p = \Delta\lambda \frac{\partial f}{\partial \boldsymbol{\sigma}'}. \tag{5}$$

In above, λ is the plastic multiplier and f is a yield function. In this study we use the Drucker-Prager failure criterion (Drucker and Prager, 1952) which is suitable for geomaterials, such as soil, ceramic and fractured rocks. The total strain tensor in Eq. (4) is the symmetric part of the deformation tensor given by

$$\boldsymbol{\varepsilon}(\mathbf{u}) = \frac{\mathbf{1}}{\mathbf{2}}\left(\nabla \boldsymbol{u} + \nabla \boldsymbol{u}^{\boldsymbol{T}}\right). \tag{6}$$

2.2 Continuity equation

The mass conservation of fluid within the porous medium is described by the continuity equation:

$$\frac{\partial \zeta}{\partial \mathrm{t}} + \nabla . \boldsymbol{q} = 0, \tag{7}$$

in which ζ is the fluid content and q is the fluid discharge given by the Darcy's law

$$\boldsymbol{q} = -\frac{k}{\mu}\nabla p, \tag{8}$$

where k is the permeability and μ is the injected fluid viscosity. The constitutive law relating the fluid content ζ and pressure p is expressed as

$$p = M\zeta - \alpha \mathrm{tr}(\boldsymbol{\varepsilon}). \tag{9}$$

Here, M is the Biot's modulus and tr (ε) is the trace of the strain tensor. In this study k is related to the plastic multiplier (λ) through an empirical correlation. The sets of initial and boundary conditions corresponding to the flow equation are:

$$\mathbf{q}.\mathbf{n}\left(\text{on } \partial\Omega_q\right) = \bar{\mathbf{q}}, \ \mathrm{p}(\text{on } \partial\Omega_p) = \bar{\mathrm{p}}, \tag{10}$$

where $\bar{\mathbf{q}}$ and $\bar{\mathrm{p}}$ are the prescribed flow and pressure on the boundary $\partial\Omega_q$ and $\partial\Omega_p$, respectively.

3. Results and discussion

In this section, we present an example of a SV simulation for a 3D hydraulic fracturing problem. Note that, the adopted numerical scheme to solve the system of the governing equations is based on the standard finite element Galerkin. It is assumed that water is injected at the wellhead flow rate of $q_{wh}=10^{-1}$ m^3/s at a center of 100m x 100m x 100m domain characterized by, initial yield stress σ_{y0} =0.2 MPa, initial porosity φ =5%, and initial virgin permeability k_0 =1 nd (Fig. 3). The characteristic length scale which controls the natural fracture distribution and the micromechanics of fracturing is l=45cm. The detail description of the characteristic length scale and its role on the SV evolution is given in Sarvaramini et al., 2017 and Sarvaramini et al. 2018. The injection is stopped at t=460s and pressure is allowed to fall-off (Fig. 3b). Note that the injection rate is specified at the surface through incorporating the wellbore storage effects in the governing equation.

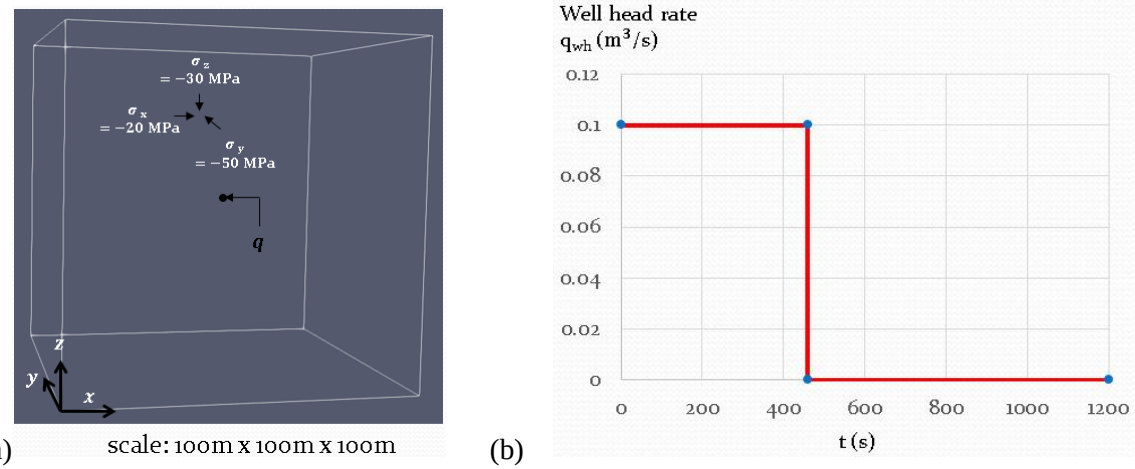

Fig. 3: Schematic of the (a) 3D injection problem, (b) wellhead rate

The domain is initially subjected to an initial stress field given by σ_{xx} (= σ_{min}) =-20 MPa and σ_{yy} (= σ_{max}) =-40 MPa, and σ_{yy} (=σ_{int}) =-50 MPa. It is assumed that the formation is not initially over/under pressurized and pore pressure is hydrostatic. The initial reservoir pore pressure is p_0=14.3 MPa. The list of other physical parameters is given in Table 1.

Table 1 Summary of the material properties

Parameter		Unit
Wellbore storage (c_w)	0.01	m^3/MPa
Wellhead rate (q_{wh})	10^{-1}	m^3/s
Initial permeability (K_0)	1	nd
Young's modulus (E)	27	GPa
Friction angle (φ)	30	°
Fluid viscosity (μ)	1	cp

Biot's coefficient (α)	1

3.1 Stimulated Volume Evolution-pre-shut-in period

The objective of this section is to quantify the evolution of the SV and associated conductivity for the injection (pre-shut-in) period. Fig. 4 shows the evolution of the non-local plastic strain (in the x-y plane) for three selected time steps, t=200s, t=350s, and t=460s (shut-in moment). As expected, SV is propagating symmetrically with respect to the injection point and it grows in the direction of the minimum principal stress, while opening against the minimum confining stress due to the principal of the work minimization as fracture needs less energy to propagate in the direction of the maximum principal stress. The "peanut" shape of the plastic damage zone is resulted from the complex tension and compression state around the injection point creating a lower shear stress environment on the broadside of the fracture perpendicular to the direction of the minimum principal stress. It is worthwhile to mention that the existence of the "peanut" shape has been previously observed in the microscale study of failure in a granular materials using the Discrete Element Approach.

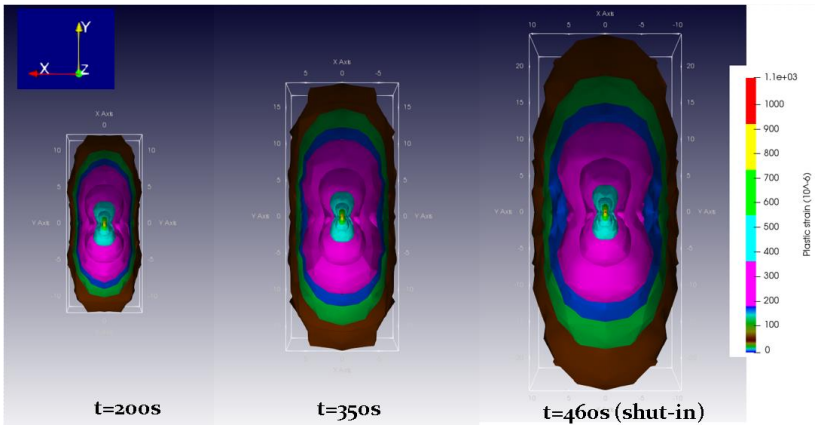

Fig. 4: Evolution of the plastic strain with time for three selected time steps, t=200s (on the left), t=350 s, and t=460s (on the right).

The evolution of the fluid pressure with time at the injection point is illustrated in Fig. 5 (Blue line). The fluid pressure initially increases to the "breakdown" pressure. This period is associated with a significant stress rise empowered by the injected fluid to overcome the initial resistance of the rock mass. Breakdown pressure is usually significantly higher than the closure stress (σ_{min}) and its value primarily depends upon the natural fracture distribution, reservoir properties, and fracturing treatment parameters. In this example, a breakdown pressure of p_B =190 MPa is inferred from the graph. After the peak point, the bottomhole pressure gradually reduces until a stabilized fracturing pressure is established. At this point, the energy required to create the propagate the SV becomes almost negligible (viscosity dominated regime). The evolution of the bottom-hole rate (sand-face) rate is also shown on the same graph. Although the wellhead rate is fixed before the moment of the shut-in, there is initially a lag before the bottom-hole rate becomes equal to the surface rate. During this period the reservoir

flow the reservoir flow period is masked by the wellbore storage effects. Similarly, the bottom hole rate, after the shut-in (at q_{wh}=0), will gradually decline until the end of the wellbore storage effects when the sand face rate becomes zero. The evolution of the SV permeability with time is also illustrated in Fig. 6.

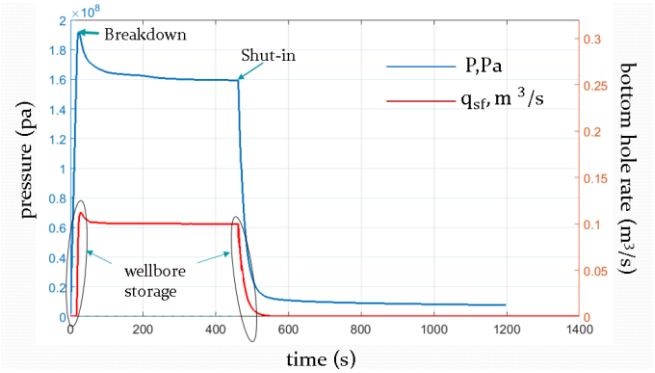

Fig. 5: The evolution of the injected bottom hole pressure (blue) and bottom hole rate (red) with time

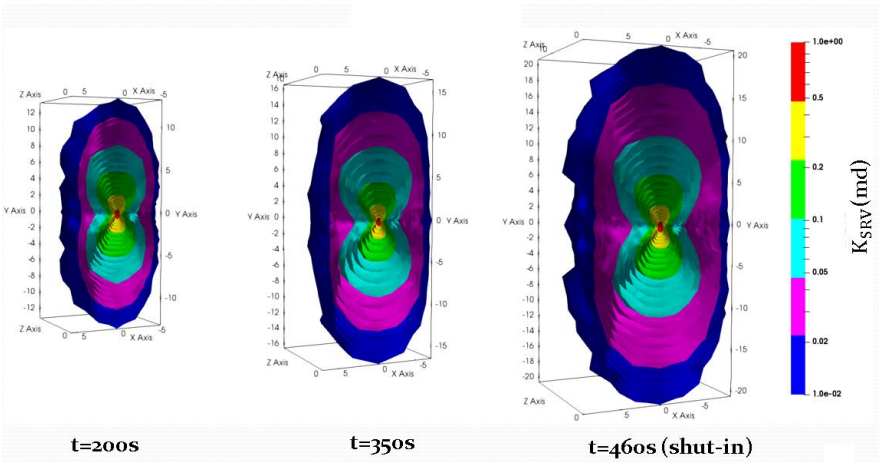

Fig. 6: Evolution of the stimulated permeability with time for three selected time steps, t=200s (on the left), t=350s, and t=460s (on the right).

3.2 Post-shut-in phase

Consider again the example of the SV evolution presented in previous section. The injection is stopped after t_s=460s and the pressure is allowed to fall-off (Fig. 5). The corresponding pressure at shut-in is p_s =158.5MPa, which in this case is equal to the stabilized fracturing propagation pressure. Fig. 7 shows the evolution of Δp (p_s-p) with Δt (t-t_s) for the pressure fall-off period. The pressure derivative type curve is also shown for comparison. Note that the pressure derivative curve in Fig. 7 is analogous to the G-function plot of a DFIT. As illustrated in Fig. 7, the pressure and derivative curves at the early period of the shut-in are characterized by a straight line of slope (m=1) suggesting that the flow regime is storage dominated. The diversion of the pressure and derivative curves from the straight line often indicates the end of wellbore and frictional effects. The most distinguished feature of the derivative

curve in Fig. 7 is the characteristic 'hump' which is indicative of the fracture closure condition. The location of this maximum point can be used to identify the fracture closure pressure. Note that the fracture closure pressure and minimum in-situ stress are identical and interchangeably used.

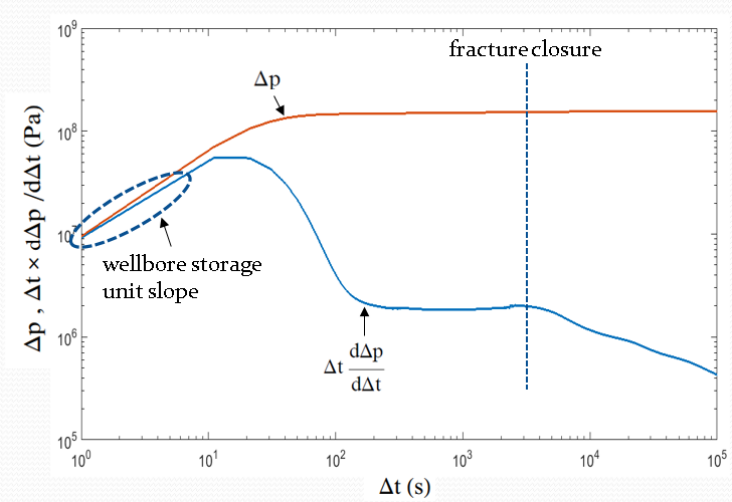

Fig. 7: Evolution of the pressure derivative type curves for the post injection shut-in analysis of a SV

For this example, we do a crosscheck on the value of the fracture closure pressure which is expected to be at $p_c = \sigma_{min}$ =20MPa. Based on the pressure derivative curve, the onset of fracture closure pressure is forecasted at $\Delta p_c = p_s - p_c$= 153.19MPa. In the view of the shut-in pressure (p_s=158.5MPa) and the initial reservoir pore pressure (p_0 =14.3MPa), the corresponding final fracture closure pressure is p_c= 19.61MPa. Note that the lack of a clear hump or closure on the semilog derivative plot can be related to the extremely low permeable nature of the rock (k_0=1nd). The low permeability of the jointed rock mass also leads to a long transitional period between the unit slop and closure condition.

4. Conclusions

In this article, we presented a new approach with the goal of simulating the Stimulated Volume evolution in the naturally fractured rocks. We first considered an example of the 3D SV evolution for a synthetic example of water injection into a tight formation. The evolution of the plastic strain and permeability with time were obtained. Next, we carried out the pressure decline analysis using the pressure and pressure derivative type curve to identify the various flow regimes of the SV. The result showed that long transitional flow period between the storage regime and fracture closure is expected due to the extremely low permeable nature of the rock mass. Additionally, no clear indication of the fracture closure and characteristic humps were observed compared to the traditional fall-off curves.

Acknowledgements

The authors gratefully acknowledge the support of a Discovery Grant and a Strategic Grant from the Natural Sciences and Engineering Research Council of Canada (NSERC) for the early stages of the research and a NSERC Discovery Grant for the later stages.

References

1. Biot M.A. 1941. General theory of three-dimensional consolidation. J. Appl. Phys., pp. 155-164.

2. Cipolla C.L., Warpinski N.R., Mayerhofer M., Lolon E.P., and Vincent M. 2010. The relationship between fracture complexity, reservoir properties, and fracture-treatment design. Society of Petroleum Engineers production and Operations.

3. Drucker D.C. and Prager W. 1952. Soil mechanics and plastic analysis or limit design. Quarterly of applied mathematics, pp. 157-165.

4. Dusseault M.B. J. McLennan, and J. Shu. 2011. Massive multi-stage hydraulic fracturing for oil and gas recovery from low mobility reservoirs in China., Petroleum Drilling Techniques, pp. 6-16.

5. Dusseault M.B. 2013. Geomechanical aspects of shale gas development. Rock Mechanics for Resources, Energy and Environment.

6. Maxwell S. Microseismic imaging of hydraulic fracturing: Improved engineering of unconventional shale reservoirs. Society of Exploration Geophysicists, 2014

7. Mayerhofer M.J., Lolon E., Warpinski N.R., Cipolla C. L., Walse D. W., and. Rightmire C. M. 2010. What is stimulated reservoir volume? Society of Petroleum Engineers production and Operations. pp. 89-98.

8. Sarvaramini E., Dusseault M.B., and R. Gracie. 2018. Characterizing the stimulated reservoir volume during hydraulic fracturing-connecting the pressure fall-off phase to the geomechanics of fracturing. Journal of Applied Mechanics (Submitted).

9. Sarvaramini E., Dusseault M.B., Komijani M., and Gracie R. 2017. A non-local plasticity model of stimulated volume evolution during hydraulic fracturing. International Journal of Solids and Structures (Submitted).